Desorption studies of metal atoms using laser-induced surface-plasmon excitation

Ida Lee,* T. A. Callcott,* and E. T. Arakawa
Health and Safety Research Division, Oak Ridge National Laboratory, Oak Ridge, Tennessee 37831-6123
(Received 26 May 1992)

Au, Al, and Ag atoms have been desorbed from thin films on glass by laser-excited surface plasmons in an attenuated-total-reflection geometry. Desorption yields are measured as a function of angle of incidence near the optimum coupling angle and the kinetic energies of desorbed neutral atoms are determined. A linear dependence of desorption yield on photon intensities and the presence of high-kinetic-energy atoms suggest that the major desorption mechanism is a nonthermal electronic process. Possible desorption processes are discussed.

I. INTRODUCTION

Photodesorption induced by laser light has been used to produce well-defined microstructure[1,2] (via micromachining), to study high-T_c superconductors[3,4] (via surface analysis), and to probe molecular dynamics in heterogeneous systems.[5,6] Studies of these processes have therefore been actively pursued in the past and are continuing with increasing sophistication.[7,8] Photodesorption of particles from a solid surface can be achieved by rapid surface heating, by coupling to phonon modes, and by coupling to an electronic excitation process. Since the basic mechanisms of electronic-excited desorption are not well understood, there has been much interest in studying this effect.

A promising new method of photodesorption based on the excitation of surface plasmons on a metal surface has been investigated recently.[9,10] The method makes use of the fact that the excitation of surface plasmons can greatly amplify the electric-field strength in the surface region. Hoheisel *et al.* have observed laser-induced desorption stimulated by surface-plasmon excitation in small metal particles.[9,11] We have observed laser-induced surface-plasmon desorption of Al atoms and rhodamine B molecules from Al films in an attenuated-total-reflection (ATR) configuration.[10,12] In the ATR geometry, photons can excite surface plasmons over a wide range of photon energies below the surface-plasmon energy. This ability to tune the wavelength will be useful in studies of electronic desorption processes.

In this study, we have measured desorption yield from Au, Al, and Ag films in an ATR geometry. We report measurements of the dependence of the desorption rate on laser fluence, on the angle of incidence of the light which determines the degree of coupling of the laser light to the plasmon mode, and relate these results to energy absorption in the film. In addition, we report measurements of the kinetic-energy distribution of the desorbed atoms. Finally, the mechanism responsible for the desorption will be discussed.

II. EXPERIMENTAL APPARATUS AND PROCEDURES

The experimental apparatus for desorption is shown in Fig. 1. The beam from the second harmonic of a Nd:YAG (yttrium aluminum garnet) laser with wavelength 532 nm and pulse length 7 ns (solid line in Fig. 1) is passed through a set of attenuation slides, a lens, mirrors, and a prism onto the sample. The prism is illuminated by *p*-polarized light which is required to excite surface plasmons. The laser fluence of the second-harmonic beam without attentuation is 140 J/cm^2, which is more than enough to desorb atoms from solid surfaces by the generation of shock waves. For our experiment the laser beam must be attenuated by several orders of magnitude to the order of 10^{-1} J/cm^2. The second-harmonic beam is focused by a lens with focal length 50 cm, which produces a spot size at the focal point of 1.2×10^{-4} cm^2. The angle of incidence can be varied by the rotatable mirror. This rotation brings the laser beam to a different and undisturbed area on the prism surface for each incident angle. The metal-coated prism is placed in the corner of the acceleration plates of the time-of-flight mass spectrometer (TOF-MS). There are three acceleration plates, two of them not shown in Fig. 1. Desorbed neutral atoms are ionized over the entrance aperture (shown in Fig. 1) of the TOF-MS by the XeCl excimer laser with a wavelength of 308 nm and a pulse length of 7 ns. The laser fluence is 8.9 J/cm^2 (or 1.3×10^9 W/cm^2). The nonresonant multiphoton ionization process can be saturated by providing powers greater than 10^8 W/cm^2 with these 10^{-8} s pulses.[13,14] The flight path of the ions in the TOF-MS is perpendicular to the plane of the figure. After passing through two apertures of the acceleration plates and an aperture above the detector, the ions are detected by an electron multiplier (EM) (signal from EM tube in Fig. 1) in the TOF-MS. The apertures are covered with 85% transparent nickel mesh to maintain a uniform field strength. These desorption experiments are performed in a cryopumped vacuum system with a base pressure of 10^{-7} Torr.

The major parts of the electronics used in this experiment are also shown in Fig. 1. The triggering device of the Nd:YAG laser is connected to a delay generator which, after a chosen time delay, will trigger the excimer laser. Varying the delay time between the two lasers allows us to measure the velocity distributions of the desorbed species. The timing sequence for this measurement needs some description. After the desorbing laser has been fired at the target, bursts of neutral atoms emit-

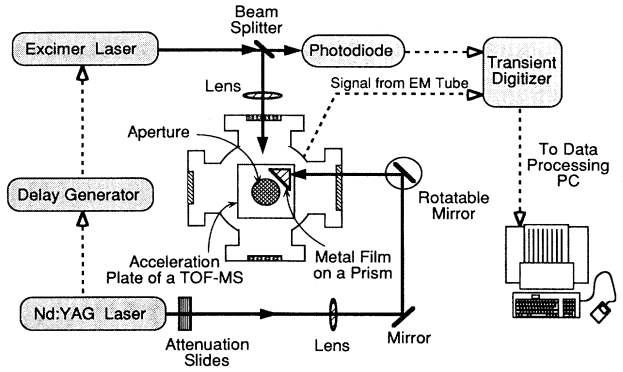

FIG. 1. Experimental apparatus for surface-plasmon-induced desorption measurements.

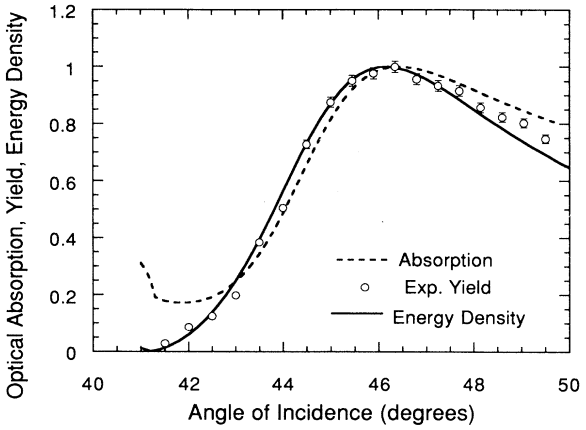

FIG. 2. Comparison of desorption yield with total optical absorption and energy density at the metal-vacuum interface for the Au film. All curves normalized to one at 47°.

ted by the target pass through the ionization region just above the extraction aperture located in the center of the acceleration plates of the TOF-MS. The desorbed particles have different translational velocities, so that the fast ones reach the ionization region earlier than the slow ones. Pulses from the ionizing laser arrive after a variable delay (0–200 μs) and are focused through the ionization region. Thus at various delay times, particles with various velocities are ionized. The Nd:YAG laser is set at a repetition rate of 10 Hz. Part of the light from the excimer laser is monitored by a photodiode which triggers the transient digitizer. This digitizer allows the user to record only the signals of interest into memory and to block out the nonimportant dead time between events. Thus the system has deep memories which permit uninterrupted recording of high-frequency signals without reducing the sample rate. The transient digitizer is controlled by an (80286) PC with mathematics coprocessor. The desorption yield in this experiment is the integrated yield produced by 100 laser pulses at the same angle and excitation spot, calculated on line by the PC during the experiment.

The prisms used in these experiments are right-angle glass (BK-7) prisms. Before the thin-film depositing, the prism is washed with microwash and deionized water, then washed with acetone and methyl alcohol in an ultrasonic cleaner. The metal thin films are deposited on the prism in a vacuum evaporator with a base pressure of 10^{-6} Torr. The thickness of the Al film in this experiment is 27 nm, the Au film is 38 nm, and the Ag film is 38 nm.

III. EXPERIMENTAL MEASUREMENTS AND RESULTS

We have observed that the three metals Au, Al, and Ag can all be efficiently desorbed from the prism at angles near the plasmon resonance angle. Since we detect very few ions in this process, the atoms desorbed from the surface are mostly neutral.

The desorption yield of Au atoms from the Au film at various angles of incidence near the plasmon excitation angle is given in Fig. 2. We calculate the optical absorption (dashed line) as we did in a previous paper.[10] Good agreement is seen between the desorption yield and energy absorbed by the Au film except near 42° where the yield goes to zero, a discrepancy that is discussed further in the next section of the paper. The good agreement indicates that the desorption yield of Au atoms depends linearly on the energy absorbed by the Au film. There is a fluence threshold at about 80 mJ/cm^2, below which the signal cannot be distinguished from the noise. The kinetic-energy distribution of the desorbed Au atoms is obtained by measuring ion yield as a function of delay time between the two lasers. Since the distance from the Au surface to the ionization region was known, we could transform the delay-time distribution to a velocity distribution and kinetic-energy distribution by a simple calculation.[15] The kinetic-energy (KE) distribution for Au atoms desorbed from the Au film is given in Fig. 3. There are two peaks, one at 0.082 eV and another one at 0.33 eV. The slow peak corresponds to a temperature of about 900 K, and is a thermal peak. The delay-time distribution of the slow peak for two laser fluences is shown in Fig. 4. At 300 mJ/cm^2, the peak is at 57 μs, which corresponds to a KE equal to 0.094 eV. At 500 mJ/cm^2, the peak is at 46 μs, which corresponds to a KE equal to 0.14 eV. The kinetic temperature variation of the

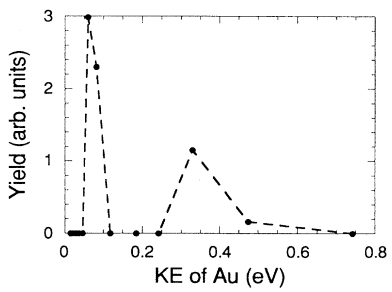

FIG. 3. Kinetic-energy distribution of Au atoms desorbed from Au film.

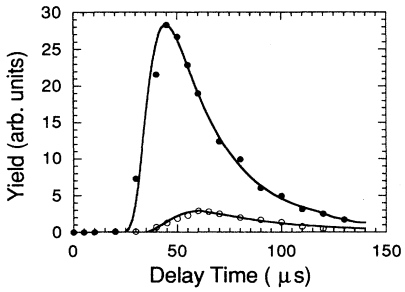

FIG. 4. The delay-time distribution of the slow peak for two laser fluences.

thermal peak with laser fluence is shown in Fig. 5. The kinetic temperature T is defined in terms of the kinetic energy of the neutral atoms by Maxwell speed distribution function

$$f(v)dv = \left[\frac{m}{2\pi kT}\right]^{3/2} \exp\left[\frac{-mv^2}{2kT}\right] 4\pi v^2 dv \ .$$

Consider the expansion of compressed, vaporized material into a vacuum,[16] where the hydrodynamic expansion velocity u is superimposed upon the thermal velocity. The detector measures the relative number of atoms at a period of drift time corresponding to the number of atoms contained within a range $(I_0+\Delta I)$. We can determine the kinetic temperature by measuring the relative number density of neutral atoms within a specified region as a function of time. Substituting $v=I/t$ and integrating over the range, we obtain

$$g(t,u) = \frac{4}{\sqrt{\pi}} \left[\frac{m}{2kT}\right]^{3/2} \times \int_{I_0}^{I_0+\Delta I} \exp\left[-\frac{m}{2kT}\left[\frac{I}{t}-u\right]^2\right] \frac{I^2 dI}{t^3} \ ,$$

where k is Boltzmann's constant and m is the mass of the appropriate metal particle. A least-squares method is used to match the experimental data for various combinations of T, u, and the data normalization constant. The kinetic temperature in Fig. 5 is then obtained by choosing the least value for the sum of squared errors. The estimated error in the kinetic temperature is 10% and is mainly due to uncertainty in the time-of-flight measurement. The slow peak moves to higher energy (or higher temperature, as shown in Fig. 5) as the laser fluence increases. The position of the high-energy peak at 0.33 eV does not vary with the laser influence.

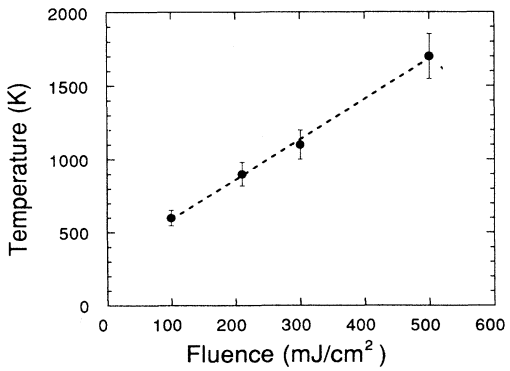

FIG. 5. Temperature variation of thermal peak with laser fluence.

There are two peaks in the kinetic-energy distribution for Al near the laser fluence threshold, one at 0.081 eV and another at 0.50 eV. For Ag, the position of the slow peak is at 0.081 eV and the position of the fast peak is at 0.90 eV. Since the translational kinetic energy of the 0.90-eV peak is very close to the detection limit ($\approx$1.0 eV) of our mass spectrometer, we turned on the deflection plates and repeated our experiment to be sure that we were not measuring the low-energy tail of a higher-energy peak. We applied a voltage of 3 eV to the deflection plates that would enable us to detect ions with KE up to 4 eV. We did not detect any particle with KE higher than 1 eV, but were still able to detect the 0.9-eV peak with slightly reduced intensity. The 0.081-eV peak cannot be detected when the deflection plates are on.

We repeated the desorption experiment with the same experimental conditions but with s-polarized laser light. We did not observe any desorption signal within the range of laser fluence from 100 mJ/cm^2 to 500 mJ/cm^2.

The results cited above are given in arbitrary units and thus provide information about relative desorption rates only. We have obtained a rough estimate of the absolute number of desorbed atoms per incident photon at the absorption maximum at the plasmon resonance angle. For the 27-nm Al film, desorption was continued until all Al was removed from the 0.1-mm^2 area of the incident beam. We find a desorption yield of $(0.2-1)\times10^{-6}$ ions/photon where the lower estimate is calculated from the average loss per pulse and the upper estimate is an extrapolated value from the desorption yield for the first few pulses. This value is comparable to the value of 7.1×10^{-6} cited by Hoheisel *et al.*[9] in their studies of plasmon-coupled desorption on rough surfaces.

The desorption results for Au, Al, and Ag are very similar. The major features may be summarized as follows:

(1) For each metal, the desorption yield follows closely the absorption curve. This implies a linear dependence of desorption on the number of photons absorbed. This linear dependence of yield on photon flux was also observed for Al by measuring the peak yield as a function of laser intensity.

(2) For each metal, the kinetic-energy distribution of desorbed atoms show two peaks, one near 0.08 eV ($\approx$900 K) that is nearly the same for each material, and a second high-energy peak of variable energy. The low-energy thermal peaks for all three metals move to higher energy as the laser intensity increase.

(3) The high-energy peaks in the kinetic-energy distribution for Au, Al, and Ag are observed at 0.33, 0.50, and 0.90 eV, respectively. These kinetic energies are four to eleven times higher than the energies of the respective

thermal peaks (Au: 4; Al: 6; and Ag: 11). The kinetic energy of the high-energy peak is independent of the laser intensity.

(4) We also observed peaks in the mass spectra from Si and SiO_2 in the prism. Both species have low-energy peaks near 0.08 eV, but do not have the high-energy peak. The observation of Si and SiO_2 in the mass spectra led us to examine the question of whether energy absorbed at the prism-film or film-vacuum interfaces was responsible for the desorption in this experiment. This question will be discussed in the following section.

(5) Desorption is observed only above a threshold of 80 mJ/cm^2 for the Nd:YAG laser fluence. The laser fluence at threshold was estimated by considering several factors including laser-beam divergence, focus of the lens, and reflectance of each of the surfaces.

IV. DISCUSSION AND CONCLUSIONS

We have observed both a low-energy thermal peak and a high-energy peak in the kinetic-energy distribution of laser-desorbed Au, Al, and Ag atoms. The various desorption mechanisms which could be responsible for the high-energy peak, namely thermal, shock waves, vibrational excitation, and electronic excitation, will be discussed in this section.

Thermal desorption varies exponentially with temperature, and the temperature varies linearly with the laser energy deposited in the material. Thus, thermal desorption yield is not linearly dependent upon the energy deposition in the material. However, we found the high-energy desorption yield to vary linearly with the energy deposited in the sample. Also in thermal desorption, the kinetic energy of the desorbed neutral should increase as the energy deposition on the sample increases. In our experiment, the kinetic energy of the high-energy peak did not change as the energy deposition was varied. These results indicate that the desorption mechanism for the high-energy peak is nonthermal.

In order to produce shock waves, the laser irradiance usually has to be above the order of 10^9 W/cm^2.[17,18] The laser irradiance we used here is on the order of 10^6 W/cm^2. Due to the interaction of the surface with the blow off material, the different desorbed neutrals produced by shock waves should have the same momentum, which depends upon the laser intensity. Neuman[19] measured the momentum for Cu, Al, steel, brass, and Ta irradiated with a 0.3-J, 50-ns laser pulse, and found that the value of the momentum varied very little for different materials. In our experiment, metal and substrate atoms do not have the same momentum (Au: 1.86×10^{-17}; Al: 0.84×10^{-17}; and Ag: 2.27×10^{-17} dyn sec). We conclude that the high-energy neutrals are not induced by shock waves.

The energies involved in vibrationally excited desorption are usually associated with the infrared spectral region and the kinetic energies of the desorbed neutrals are usually much lower than that observed in thermal desorption. In this experiment, a visible laser (532 nm) was used for the desorption and the kinetic energy of the high-energy peak was much higher than in thermal desorption. We can therefore rule out vibrationally excited desorption as the mechanism for the high-energy peak.

In electronic-excited desorption, the desorption yield is expected to increase linearly with fluence until the thermal effect takes over. In addition, the kinetic-energy distribution of the desorbed species should remain the same for different laser fluence. These are the characteristics observed in our data which indicate that the desorption mechanism in our experiment is electronic-excited desorption. It is possible that the final state of the atoms involved in the electronic transition is vibrationally excited as in the well-known Franck-Condon excitation.

Since Si and SiO_2 were also detected in the desorption products, we examined the possibility that desorption was associated with energy absorption at the substrate-film interface rather than within the film. We calculated the electromagnetic energy density distribution inside a thin film. We can evaluate the electromagnetic energy density in a thin film by the following method. We first consider the reflection and transmission of electromagnetic radiation at a thin dielectric layer between two semi-infinite media. All the media are homogeneous and isotropic. If we assume a plane wave is incident from medium 0 (glass) through medium 1 (metal) to medium 2 (air), the whole structure can be described by the indices of refraction

$$n(x)=\begin{cases} n_0, & x<0 \\ n_1, & 0<x<d \\ n_2, & x>d \end{cases}.$$

If the plane of incidence is the xz plane, the electric-field vector of a plane-wave solution of the wave equation can be of the form

$$\mathbf{E}(x)\exp[i(\omega t-\beta z)],$$

since the medium is homogeneous in the z direction. The parameter β is the z component of the propagation wave vector. The electric-field vector can be written as

$$E(x)=\begin{cases} Ae^{-ik_{0x}x}+Be^{ik_{0x}x}, & x<0 \\ Ce^{-ik_{1x}x}+De^{ik_{1x}x}, & 0<x<d \\ Fe^{-ik_{2x}(x-d)}, & x>d \end{cases},$$

where we assume that the electric-field vector is p polarized (i.e., parallel to the plane of incidence). The complex amplitudes A, B, C, D, and F are constants, and k_{0x}, k_{1x}, and k_{2x} are the x components of the wave vectors

$$k_{ix}=\left[\frac{\omega}{c}\right]n_i\cos\theta_i, \quad i=0,1,2,$$

where θ_i is the ray angle measured from the x axis. The constant A is the amplitude of the incident wave. The constants B and F are amplitudes of the reflected and transmitted waves, respectively. For a p wave, the electric field $\mathbf{E}(x)$ is $\mathbf{z}E(x)$, and the y component of the magnetic field is obtained by using $H_y=-(i/\omega\mu)(\partial E/\partial x)$. Thus,

$$H_y(x)=\begin{cases} -\frac{k_{0x}}{\omega\mu}(Ae^{-ik_{0x}x}-Be^{ik_{0x}x}), & x<0 \\ -\frac{k_{1x}}{\omega\mu}(Ce^{-ik_{1x}x}-De^{ik_{1x}x}), & 0<x<d \\ -\frac{k_{2x}}{\omega\mu}Fe^{-ik_{2x}(x-d)}, & x>d\ , \end{cases}$$

where μ is the magnetic permeability constant. Imposing the continuity of E_z and H_y at the interfaces of $x=0$ and $x=d$, we can obtain four equations. These four equations can be used to solve for B, C, D, and F in terms of A (the amplitude of incident wave). After a few steps of algebraic manipulation and substituting the Fresnel reflection coefficient r_{12} and phase change β into the equation, we can obtain the relation between C and D as

$$D=r_{12}e^{-2i\beta}C\ .$$

By knowing the field amplitudes, the electric-field distribution in the thin films can be written as

$$E(x)=C(e^{-ik_{1x}x}+r_{12}e^{-2i\beta}e^{ik_{1x}x}),\quad 0<x<d\ .$$

The density of the relative electromagnetic energy as a function of the distance from the medium 0 (glass) can then be evaluated by using the equation

$$U(x)=\tfrac{1}{2}\varepsilon|E(x)|^2\ .$$

In Fig. 6, the energy densities inside and outside the Au film are plotted for angles near the angle of surface-plasmon excitation. At the resonant angle there is an electromagnetic field enhancement on the film-vacuum interface; the energy density there is much larger than the energy density at the prism-film interface. This indicates that the electronic energy deposition leading to desorption is most likely to take place at the film-vacuum interface. The lack of a high-energy peak for Si and SiO_2 also indicates that the electronic excitation takes place at the film-vacuum interface.

In Fig. 2, we compare the experimental desorption yield of Au with the total energy absorption in the film (dashed line) which is proportional to the area under the energy density curves within the film, and with the energy density at the film-vacuum interface (solid line), and find that the yield agrees better with the energy density. This is particularly true at angles just below the plasmon angle where both the yield and energy density go to near zero. In this region most of the absorption occurs at the substrate-film interface and does not effectively contribute to the desorption yield. These results show that indeed electronic-excited desorption occurs at the film-vacuum interface. The cohesive energies of Au, Al, and Ag are 3.38, 3.34, and 2.96 eV. The kinetic energies we measured for Au, Al, and Ag are 0.33, 0.5, and 0.9 eV which are inversely proportional to the cohesive energies. For a fixed plasmon energy input, higher cohesive energy corresponds to the lower kinetic energy. The plasmon energies and kinetic energies do not add up to the

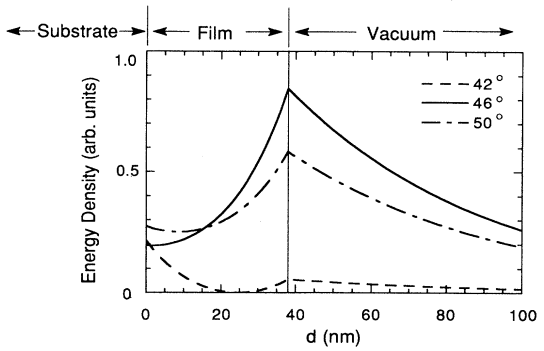

FIG. 6. Energy densities of the electromagnetic field from laser light at three incident angles. The plasmon resonance angle is 46°

cohesive energies. This is possible due to the desorption of particles from a loosely bounded site or a defect site.

Monreal and Apell[20] presented a theoretical description of the surface-plasmon-induced desorption in a small metal particle. They describe a process in which surface-plasmon excitation leads to a large field enhancement at the small-particle surface which induces electron-hole pairs, and these bonding-antibonding pairs then lead to desorption. For our desorption mechanism, a similar theory proposed by Wu[21] provides a possible mechanism. The basic assumption used by Wu is that the electronic excitation can be trapped in surface defect sites in a metal surface. Steinruck, Rendulic, and Winkler[22] have shown that in a real Ni surface, adsorption and desorption are completely controlled by surface defects. Rendulic[23] observed a shift of the hydrogen desorption peak towards lower temperatures by about 50 K from a moderately defective (surface defect concentration $\leq 5\%$) Ni surface. The influence of foreign atoms is similar to defects which reduce the sticking coefficient of adsorbed species. In our experiment, surface plasmons may produce electron-hole pairs near surface defects, which would lead to a decrease in the lattice force constant. Particles at these less tightly bound regions might then produce ions through Auger decay. The crossing of the ion-antibonding curve and atom-antibonding curve could then lead to ion neutralization and subsequent desorption of neutrals. This model can be tested by further experiment using epitaxial growth of a metal film with controlled surface defects (steps, point defects, and impurities of foreign atoms) on a single crystal in order to examine defect-related desorption more closely.

We have shown that the desorption in our experiment is neither laser-induced thermal desorption nor vibration-excited desorption. Our experimental results indicate that the desorption is electronic-excited desorption. We have also shown that the desorption was associated with energy absorption at the film-vacuum interface rather than the substrate-film interface. The desorption yield agrees better with the energy density at the film-vacuum interface than the total absorption in the film. It is therefore concluded that the plasmon excitation is not

damped by coupling to the phonon modes, but that a different deexcitation channel exists. Since evidence exists for electronic-excited desorption, the deexcitation channel appears to induce bond rupture of the metal overlayer.

ACKNOWLEDGMENTS

This work was supported by the U.S. Department of Energy under Contract No. DE-AC05-84OR21400 with Martin Marietta Energy System, Inc.

---

*Also at Department of Physics and Astronomy, University of Tennessee, Knoxville, TN 37996-1200.

[1]I. W. Boyd, *Laser Processing of Thin Films and Microstructures* (Springer-Verlag, New York, 1987).

[2]F. A. Houle, Appl. Phys. A **41**, 315 (1986).

[3]J. B. Pallix, C. H. Becker, and N. Newman, J. Vac. Sci. Technol. A **6**, 1049 (1988).

[4]C. H. Becker and J. B. Pallix, J. Appl. Phys. **64**, 5152 (1988).

[5]T. T. Tsong, Phys. Rev. B **30**, 4946 (1984).

[6]R. Tembreull and D. M. Lubman, Anal. Chem. **58**, 1299 (1986).

[7]T. J. Chuang, Surf. Sci. **178**, 763 (1986).

[8]H. Zacharias, Appl. Phys. A **47**, 37 (1988).

[9]W. Hoheisel, K. Jungmann, M. Vollmer, R. Weidenauer, and F. Trager, Phys. Rev. Lett. **60**, 1649 (1988).

[10]I. Lee, J. E. Parks II, T. A. Callcott, and E. T. Arakawa, Phys. Rev. B **39**, 8012 (1989).

[11]W. Hoheisel, U. Schulte, M. Vollmer, R. Weidenauer, and F. Trager, Appl. Surf. Sci. **36**, 664 (1989); R. Weidenauer, M. Vollmer, W. Hoheisel, U. Schulte, and F. Trager, J. Vac. Sci. Technol. A **7**, 1972 (1989); M. Vollmer, R. Weidenauer, W. Hoheisel, U. Schulte, and F. Trager, Phys. Rev. B **40**, 12 509 (1989); W. Hoheisel, U. Schulte, M. Vollmer, and F. Trager, Appl. Phys. A **51**, 271 (1990).

[12]I. Lee, T. A. Callcott, and E. T. Arakawa, Anal. Chem. **64**, 476 (1992).

[13]C. H. Becker and K. T. Gillen, Anal. Chem. **56**, 1671 (1984).

[14]C. H. Becker and K. T. Gillen, J. Opt. Soc. Am. B **2**, 1438 (1985).

[15]N. S. Nogar, R. C. Estler, and C. M. Miller, Anal. Chem. **57**, 2441 (1985).

[16]C. Peugnet, J. Appl. Phys. **48**, 3206 (1977).

[17]J. F. Ready, *Effects of High-Power Laser Radiation* (Academic, New York, 1971).

[18]Yu. A. Bykovskii, V. G. Degtyarev, N. N. Degtyarenko, V. F. Elesin, I. D. Laptev, and V. N. Nevolin, Zh. Tekh. Fiz. **42**, 658 (1972) [Sov. Phys. Tech. Phys. **17**, 517 (1972)].

[19]F. Neuman, Appl. Phys. Lett. **4**, 167 (1964).

[20]R. Monreal and S. P. Apell, Phys. Rev. B **41**, 7852 (1990).

[21]Z. Wu, Phys. Lett. A **131**, 486 (1988); L. Chen, V. Liberman, J. A. O'Neill, Z. Wu, and R. M. Osgood, Jr., J. Vac. Sci. Technol. A **6**, 1426 (1988).

[22]H. P. Steinruck, K. D. Rendulic, and A. Winkler, Surf. Sci. **29**, 99 (1985); H. P. Steinruck, A. Winkler, and K. D. Rendulic, *ibid.* **152/153**, 323 (1985).

[23]K. D. Rendulic, Appl. Phys. A **47**, 55 (1988).